CHEMISTRY
A European Journal

A Journal of
ChemPubSoc Europe

Accepted Article

Title: All-in-one: Electroactive Nanocarbon as Simultaneous Platform and Label for Single-step Biosensing

Authors: Zhao Xuan Cheng and Alessandra Bonanni

To be cited as: *Chem. Eur. J.* 10.1002/chem.201705729

Link to VoR: http://dx.doi.org/10.1002/chem.201705729

Supported by
ACES

WILEY-VCH

10.1002/chem.201705729

All-in-one: Electroactive Nanocarbon as Simultaneous Platform and Label for Single-step Biosensing

Zhao Xuan Cheng and Alessandra Bonanni*

Division of Chemistry & Biological Chemistry, School of Physical and Mathematical Sciences, Nanyang Technological University, Singapore 637371

Fax: (65) 6791-1961

Email: a.bonanni@ntu.edu.sg

*Author for correspondence

10.1002/chem.201705729

Abstract

We demonstrate here that an electroactive nanocarbon material can simultaneously work as both platform and label for the detection of mycotoxins. The versatility of the material for the immobilization of biorecognition elements was combined with its ability to provide an intrinsic electrochemical signal upon reduction of the oxygen functionalities on its surface. The intensity of peak current reflects the availability of oxygen functionalities for reduction, which can be directly correlated to the specific biorecognition event. We show that the use of electroactive nanocarbon as all-in-one biosensing component enables sensitive quantification of Fumonisin B_1 (FB_1) as model mycotoxin analyte, but it can be easily implemented to develop label-free, cost-effective and fast bioanalytical devices for universal biosensing.

1. Introduction

Recent years have witnessed the upsurge of electroactive nanomaterial applications to biosensing. Metal nanoparticles, semiconductor quantum dots, and 2D layered nanomaterials have been employed as electroactive labels in a cost-effective and more promising alternative to optical detection.[1-8] The working signal, arising from the electrochemical oxidation or reduction of the electroactive nanomaterial used as label has been subsequently correlated to the presence and amount of the specific analyte. Electroactive carbon nanomaterials such as nano-graphene oxide have shown great promises as electrochemical labels for the detection of biomolecules. Specifically, the presence of oxygen containing groups (OCGs) such as hydroxyl, peroxy, epoxy, carbonyl, carboxyl, ether and ester groups distributed along the surfaces and at the edges of the graphene sheets,[9-10] enables the material to become extremely electroactive.[11-13] Particularly useful is the presence of electrochemically reducible oxygen groups, which generate intrinsic electrochemical signals that can be exploited for biosensing applications. In fact, inherently electroactive graphene oxide nanoplatelets have been successfully used as signalling labels for biosensing.[14-16]

Furthermore, due to the large surface area and abundance of OCGs, graphene oxide has also been commonly utilized as platform for the immobilization of bio-molecules by physical adsorption, covalent coupling, or affinity interactions.[17-19]

In view of these exceptional features shown by graphene oxide, and considering the cost effective production of bulk amounts from graphite oxidation,[20-23] we propose here the use of graphene oxide nanocolloids (GONCs) as our electroactive nanocarbon material with the double function of both immobilizing platform and signalling label at the same time. This new concept, where the quantifying signal arises directly from the platform rather than the label, enables the development of a label-free biosensor requiring only single-step operations once the material has been modified with the biorecognition element. Herein, we wish to use this model for the development of an aptasensor for the detection of Fumonisin B_1 (FB_1), a highly carcinogenic mycotoxin.[24-25]

The rationale behind the biosensor design is based on the variation of GONC electroactivity at each step of the biosensing. Once the DNA aptamer serving as the biorecongnition element is immobilized on GONC surface by physical adsorption, non-covalent interactions involving both the graphene sp^2 network and OCGs take place. These interactions alter the electroactivity of the material, since the oxygen groups involved become less available for reduction. In the presence of the target analyte, the aptamer-mycotoxin conjugate is formed. As a consequence, the OCGs on the platform are released from the above mentioned interactions, and a partial restoration of the original electroactivity of the material is observed. We demonstrate a direct correlation between the biorecognition event and the changes in electroactivity of the electroactive nanocarbon platform, enabling precise quantification of the analyte under investigation and good selectivity.

2. Experimental

2.1 Materials

Graphene oxide nano-colloids (GONCs), Fumonisin B_1 aptamers (FB_1-Apt) [5'-CGATCTGGATATTATTTTTGATACCCCTTTGGGGAGACAT-3'], Ochratoxin A (OTA), Fumonisin B_1 (FB_1), thrombin (THR), sodium chloride (NaCl), sodium phosphate dibasic salt (Na_2HPO_4), tris(hydroxymethyl)aminomethane [$NH_2C(CH_2OH)_3$] (Tris), potassium hexacyanoferrate (II) trihydrate ($K_4[Fe(CN)_6].3H_2O$), and potassium hexacyanoferrate (III) ($K_3[Fe(CN)_6]$) were purchased from Sigma-Aldrich (Singapore). Ultrapure water for all experiments was attained using Milli-Q ion-exchange column (Millipore) with resistivity of 18.2 MΩ cm.

Buffer solutions used in the experiments were: PBS (0.01 M Na_2HPO_4; 0.1 M NaCl; pH 7.2) and Tris (0.025 M Tris; 0.3 M NaCl; pH 8.2). GONCs were diluted using ultrapure water (1 mg/mL), and ultrasonicated for 5 minutes at room temperature to obtain GONCs homogeneous dispersion.

Disposable electrical printed (DEP) carbon electrodes were purchased from BioDevice Technology (Nomi, Japan). Each unit comprises a three-electrode system, inclusive of a carbon-based working and counter electrodes, and an Ag/AgCl reference electrode.

2.2 Equipment

Differential pulse voltammetry (DPV), cyclic voltammetry (CV), and electrochemical impedance spectroscopy (EIS) measurements were performed using μAutolab type III electrochemical analyzer (Eco Chemie, Utrecht, The Netherlands) connected to a computer. DPV measurements were controlled using General-Purpose Electrochemical System (GPES) software version 4.9, and the parameters applied for GONC reduction were the following: 0.05 s modulation time, 0.5 s interval time, 0.01 V step potential, 0.05 V modulation amplitude, and 0.05 V/s scan rate. DPV measurements were conducted using PBS buffer solution, with the raw data corrected with a baseline correction of peak width 0.026 by using the GPES software. The parameters applied for guanine oxidation were following: 0.05 s modulation time, 0.5 s interval time, 0.025 V modulation amplitude and 0.005 V step potential. The raw data were corrected with a baseline correction of peak width 0.026 using the GPES software.

CV measurements were controlled using General-Purpose Electrochemical System (GPES) software, version 4.9, and the parameter applied were 5 s equilibrium time, 0.00167 V step potential and 0.05 V/s scan rate. CV measurements were conducted in PBS buffer solution.

Impedance measurements were controlled using Frequency Response Analyzer (FRA) and recorded with 5 s equilibrium time. Impedance measurements were performed using 10 mM $K_4[Fe(CN)_6]$/ $K_3[Fe(CN)_6]$ (1:1 molar ratio) in PBS buffer solution as the redox probe, in a frequency range from 0.1

MHz to 0.1 Hz, and with modulation amplitude of 10 mV. Randles equivalent circuit was used to fit the obtained impedance spectra, which were presented as Nyquist plots in the complex plane.
All washing steps and incubation of both analyte and negative controls were performed using TS-100 thermo-shaker (Biosan, Riga, Latvia).
XPS (X-ray photoelectron spectroscopy) was carried out with a Phoibos 100 spectrometer including a monochromatic Mg X-ray radiation source (SPECS, Germany).
STEM micrographs were obtained with a 30 kV scanning electron microscope (Jeol 7600F, Japan).

2.3 Procedures

GONCs was immobilised on the DEP electrode surface through dry physical adsorption. GONC solution (3µL) at concentration of 1 mg/mL was casted onto the clean, bare electrode surface and dried under a lamp. FB_1-apt was subsequently immobilized on the GONC platform through physical absorption. FB_1-apt in PBS buffer solution at optimum concentration of 10 µM (3µL) was cast onto the GONC platform and dried in oven at 60°C for 10 minutes. The electrodes were then washed in PBS buffer solution for 5 minutes at 25°C with gentle stirring to remove the excess aptamers which were non-specifically adsorbed on the surface of the electrodes. The FB_1-apt modified DEP electrodes were then incubated in Eppendorf tubes with the targeted concentration of FB_1, OTA or THR in Tris buffer solution (100µL). The incubation step was carried out for 1 h at 37°C with gentle stirring. Two washing steps were subsequently conducted in Tris buffer solution at 37°C for 5 min each.

3. Results and Discussion

GONCs are proposed here as the electroactive nanocarbon material to serve for the first time as both platform for the immobilization of the biorecognition element, and also label that provides the electrochemical signal for biosensing. This can be achieved because of the inherent electroactivity of GONCs, which produces a large reduction peak arising from the electrochemically reducible oxygen containing groups (OCGs) when potential is cathodically scanned.[11, 26]
Figure 1 shows a scheme of the experimental protocol for biosensing, and the principle for working signal measurement using GONCs as platform and label for biosensing. Bare GONCs immobilized on the electrode surface and carrying electroactive OCGs are firstly tested to measure the reducing signal arising from the reduction of electrochemically reducible oxygen functionalities (see Figure 1A, grey line).
When the same measurement is carried out after the immobilization of FB_1-Apt as the biorecognition element, a significant decrease of the electrochemical signal is observed (see Figure 1B, blue line). This

10.1002/chem.201705729

is due to the formation of non-covalent interactions including hydrophobic, hydrogen bonds and π-π interactions between GONC surface and FB_1-Apt,[27-28] leading to a diminished amount of OCGs available for reduction.

Upon incubation with Fumonisin B_1 (FB_1), specific binding occurring between the FB_1-Apt and the FB_1 lead to the conformational alteration and subsequent detachment of the immobilized FB_1-Apt from GONC surface.[15-16, 29-30] This generates an increase in the amount of OCGs available for reduction, therefore partially restoring the original GONC inherent electroactivity (see Figure 1C red line). Differential pulse voltammetry (DPV) with cathodic potential scanning is used instead of cyclic voltammetry as significantly enhanced electrochemical signal is generated, thus providing a more sensitive quantification.

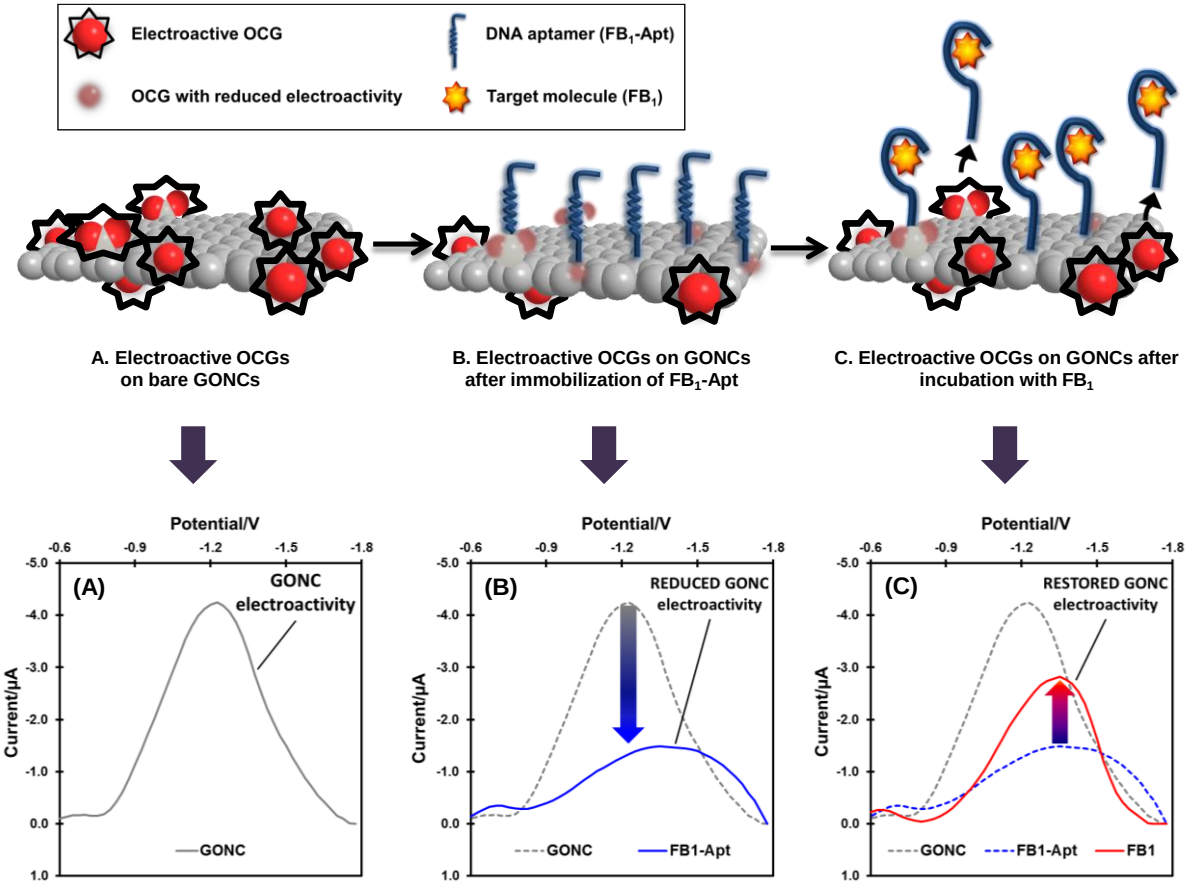

Figure 1. Scheme showing the utilization of GONCs as platform for transduction and signal generation for the detection of Fumonisin B_1. A: Electroactivity of bare GONCs is first measured providing a reduction peak due to the presence of electrochemically reducible OCGs on GONC surface. B. After immobilization of FB_1-Apt, electroactivity of GONC surface is reduced due to the formation of non-covalent interactions between FB_1-Apt and OCGs on GONC surface. C. After incubation with FB_1, the FB_1-Apt/FB_1 complex is formed and partially released from GONC surface; a restored electroactivity is observed, due to diminished interactions between FB_1-Apt and OCGs on GONC surface.

This mechanism was confirmed by electrochemical impedance spectroscopy (EIS) measurement performed on GONC surface after each step of biosensing (see Figure S1 of Supporting Information). The impedimetric signal, recorded as Nyquist plot in the complex plane, showed an increase in the charge transfer resistance (R_{ct}) after modification of GONCs with FB_1-Apt. This is due to the repulsion between the negatively charged $[Fe(CN)6]^{3-/4-}$ used as redox probe and the similarly charged phosphate backbone of FB_1-Apt. In addition, the steric hindrance introduced with the immobilization of FB_1-Apt on GONC surface also contributes to an overall R_{ct} increase. In contrast, a decrease in R_{ct} value was recorded after incubation with FB_1. These measurements together with the variation of GONC inherent electroactivity provide evidence that the formation of FB_1-Apt / FB_1 conjugate results in the partial detachment of the probe from the GONC surface, which explains the decrease in R_{ct} found in EIS study, and the restored reduction peak from GONC electroactivity found in DPV study.

Electrochemical and chemical characterization of GONCs was preliminarily performed in order to ascertain the presence of oxygen functionalities and the inherent electroactivity of the material. Cyclic voltammetry can easily verify the presence of OCGs that are electrochemically reducible, which is a necessary condition for the material to be employed. As depicted in Figure 2A, when the potential is scanned from 0 V to -1.8 V, a large reduction peak is observed only during the first scan of the GONC-modified electrode. This signal is not reproduced during the subsequent second and third scans. This experiment shows that i) a significant amount of electrochemically reducible OCGs is present on the GONC material and ii) these are fully reduced upon one reducing potential scan. [13-16] The corresponding differential pulse voltammetric (DPV) peak is shown in Figure S2 of Supporting Information, being DPV the technique used is this study due to its superior sensitivity. XPS analysis can provide information on the type and amount of the different OCGs present on the GONC surface. C 1s high-resolution XPS spectrum is presented in Figure 2B. It can be seen that the C 1s spectrum can be deconvoluted into four prominent signals at different binding energy values. The signal observed at 284.5 eV can be attributed to the C=C sp^2 carbon bond; the peak at 286 eV is associated with C–O single bond, while the higher energy tails at 288.4 eV and 289.5 eV are attributed to the C=O bond in carbonyl and carboxyl groups, respectively. XPS results showed a high degree of oxidation for GONC material, resulting in a C/O ratio of 1.3 as derived by the survey XPS spectrum (see Figure S3 of Supporting Information). This value is considerably lower than typical values obtained for GO which generally range between 2 and 4.[31-33] This confirms the high suitability of the material for the present study.

Furthermore, STEM characterization of GONCs was performed (see Figure S4 of Supporting Information), showing well dispersed nanocolloids with lateral size in the nanometer range.

10.1002/chem.201705729

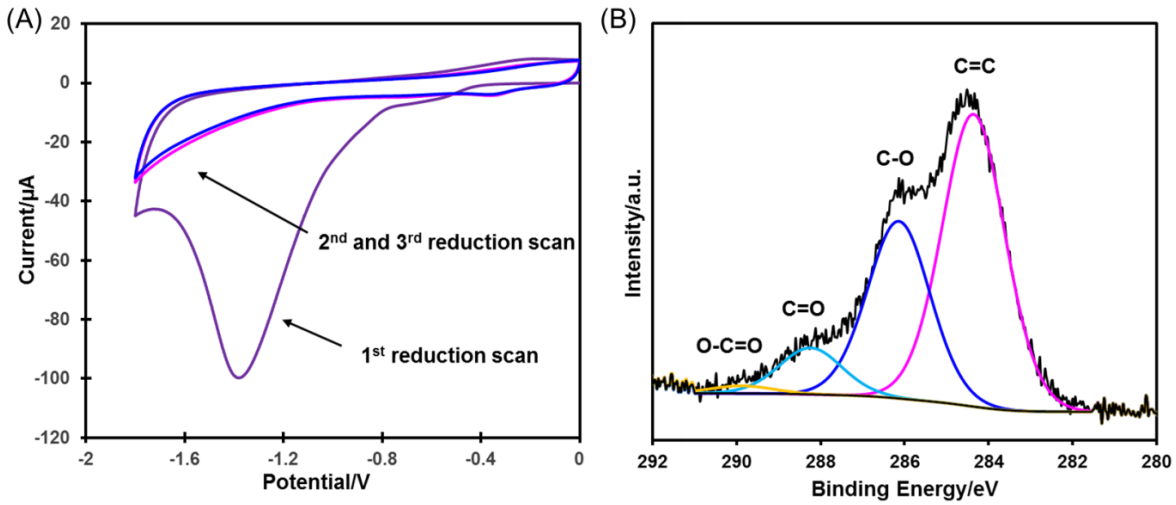

Figure 2. A. Electrochemical characterization of GONCs: cyclic voltammograms showing inherent electroactivity of GONCs due to the presence of electrochemically reducible OCGs. B. X-ray photoelectron spectroscopy: C1s high resolution spectrum for GONCs.

Having demonstrated the ability of GONC to simultaneously act as platform and electroactive label for the detection of the specific target FB_1, we then proceeded with the optimization of the developed platform. Fumonisin B_1 aptamer (FB_1-Apt) that serves as the biorecognition element was optimized with the purpose of determining the optimum concentration to be immobilized on GONC surface. Impedance spectra were recorded after immobilization of FB_1-Apt, and results were displayed in Figure 3A. It was observed that R_{ct} vales increased upon increasing FB_1-Apt concentration. Therefore, the magnitude of the impedimetric signal indicates the amount of FB_1-Apt which has been successfully immobilized on GONC surface. Hence, the value of 10 μM was chosen to ensure the maximum GONC surface coverage.

10.1002/chem.201705729

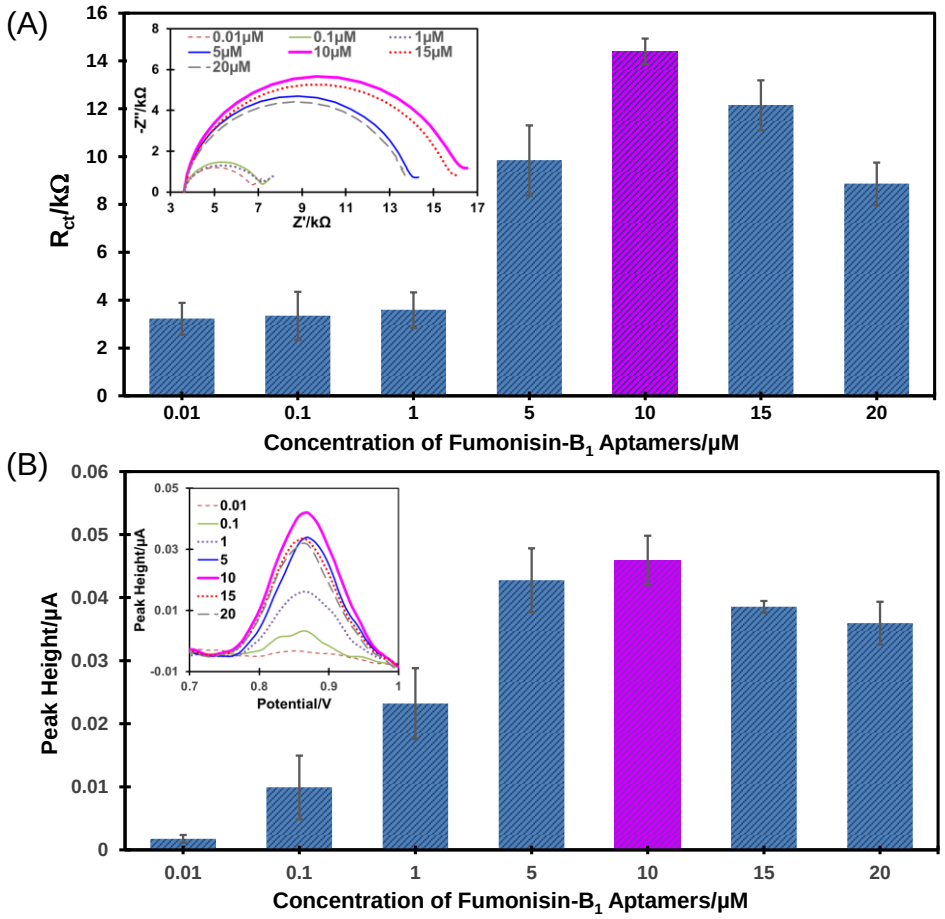

Figure 3. Optimization of FB_1-Apt concentration. A. Bar chart representing the charge transfer resistance variation towards FB_1-Apt concentration (inset showing Nyquist plots depicting imaginary impedance *-Z''* vs real impedance *Z'* for increasing FB_1-Apt concentrations). B. Bar chart representing the peak height variation for guanine oxidation towards FB_1-Apt concentration (inset showing differential pulse voltammograms for guanine oxidation at increasing FB_1-Apt concentrations).

In order to confirm the impedimetric results, a similar study was conducted by measuring guanine oxidation signal after the immobilization of FB_1-Apt increasing concentrations. Given guanine abundance in FB_1-Apt, the magnitude of oxidation peak can be easily correlated to the amount of FB_1-Apt successfully immobilized on GONC surface. From the bar chart in Figure 3B it is observed that when increasing FB_1-Apt concentration, a corresponding increase in guanine oxidation peak was recorded, confirming the maximum GONC surface cover at 10 μM FB_1-Apt, as previously obtained from EIS study.

Subsequently, in order to ascertain the detection range for GONC platform, we studied the variation of GONC reduction signal towards FB_1 concentration. Increasing concentrations of FB_1 were incubated on GONC surface modified with 10 μM FB_1-Apt, and the reduction signal for electroactive OCGs was

10.1002/chem.201705729

monitored. As depicted in Figure 4A, the formation of FB_1-Apt/FB_1 conjugate and its partial detachment from GONC surface lead to a restoration of GONC electroactivity with a consequent increase in the reduction peak current. Upon increasing FB_1 concentration an increase in the reduction current was observed with a linear dynamic range between 15 nM and 0.5 μM.

In order to verify the selectivity of the FB_1 aptasensor, control experiments were performed incubating the FB_1-Apt modified GONC with Ochratoxin A (OTA) and thrombin as negative controls. These molecules have been selected considering that OTA is another natural carcinogenic mycotoxin,[34] and thrombin is a standard protein which exhibits high affinity for aptamer binding.[15, 29] As depicted in the bar chart of Figure 4B, the signal variation in the presence of either OTA or thrombin is negligible as compared to that of FB_1, thus confirming the high selectivity of the developed biosensor towards FB_1.

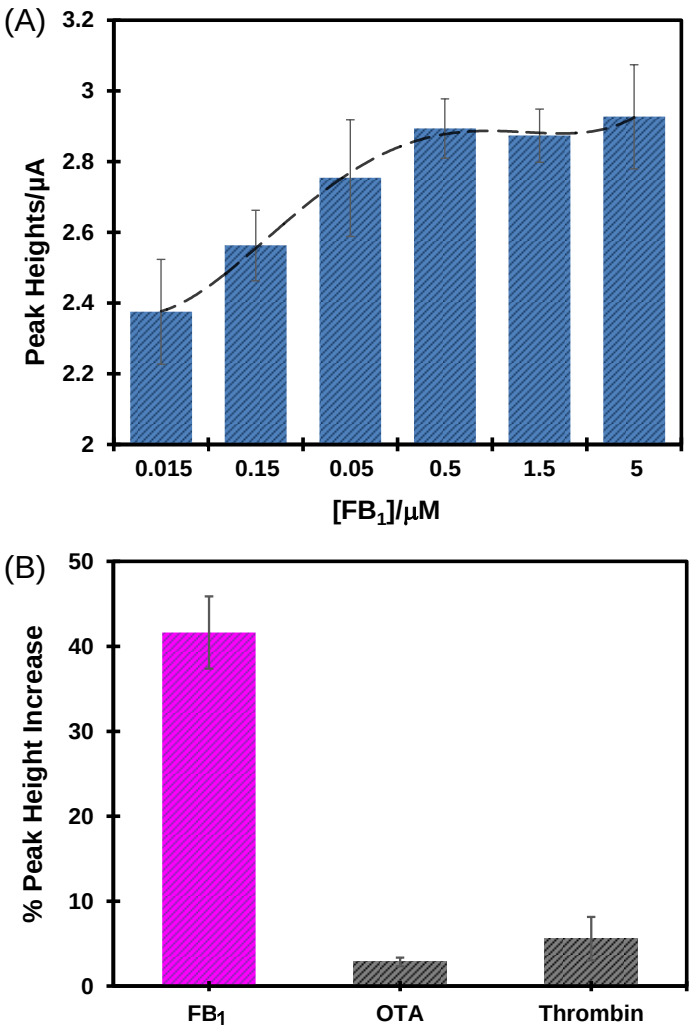

Figure 4. A. Bar chart representing the variation of GONC reduction peak towards FB_1 concentration. B. Selectivity study showing the relative increase of GONC reduction peak in the presence of FB_1 0.5 μM (positive control), OTA 0.5 μM, and Thrombin 50 nM (negative controls). FB_1-Apt concentration was kept at 10 μM.

10.1002/chem.201705729

4. Conclusions

This study successfully demonstrates the possibility to employ GONCs as electroactive nanocarbon material with the double function of transducing platform for Fumonisin B_1 aptamer (FB_1-Apt) conjugation, and at the same time acting as electroactive label for the detection of Fumonisin B_1 (FB_1) mycotoxin. The innovative approach is based on the variation in the availability for electrochemical reduction of oxygen containing groups (OCGs) on GONC surface with the specific biorecognition event between the aptamer and the target FB_1 analyte. The OCGs reduction signal is firstly decreased after the immobilization of FB_1-Apt as biorecognition element, and then partially restored in the presence of the analyte FB_1 due to detachment of FB_1-Apt/ FB_1 conjugate from GONC surface. We have shown that the electrochemical signal arising from GONC inherent electroactivity can be directly and selectively correlated to FB_1 concentration within a wide linear dynamic range from 15 nM to 0.5 uM. These findings could be easily generalized and applied to the development of compact and label-free electrochemical devices, for single-step detection in the assessment of food safety or for point-of-care diagnosis.

Acknowledgments

A. B. acknowledges Tier 1 grant (01/17) from the Ministry of Education (Singapore) and Nanyang Technological University for the financial support.

Conflict of interest

The authors declare no conflict of interest.

References

[1] S. A. Lim and M. U. Ahmed, *RSC Adv* **2016**, *6*, 24995-25014.
[2] R. Sharma, K. V. Ragavan, M. S. Thakur and K. Raghavarao, *Biosens Bioelectron* **2015**, *74*, 612-627.
[3] C. Cheng, S. Li, A. Thomas, N. A. Kotov and R. Haag, *Chem Rev* **2017**, *117*, 1826-1914.
[4] W. Tan, M. J. Donovan and J. Jiang, *Chem Rev* **2013**, *113*, 2842-2862.
[5] M. Labib, E. H. Sargent and S. O. Kelley, *Chem Rev* **2016**, *116*, 9001-9090.
[6] E. Paleček and M. Bartošík, *Chem Rev* **2012**, *112*, 3427-3481.
[7] E. Paleček, J. Tkáč, M. Bartošík, T. Bertók, V. Ostatná and J. Paleček, *Chem Rev* **2015**, *115*, 2045-2108.
[8] J. Shen, Y. Li, H. Gu, F. Xia and X. Zuo, *Chem Rev* **2014**, *114*, 7631-7677.
[9] D. R. Dreyer, A. D. Todd and C. W. Bielawski, *Chem Soc Rev* **2014**, *43*, 5288-5301.
[10] D. R. Dreyer, S. Park, C. W. Bielawski and R. S. Ruoff, *Chem Soc Rev* **2010**, *39*, 228-240.
[11] M. Zhou, Y. L. Wang, Y. M. Zhai, J. F. Zhai, W. Ren, F. A. Wang and S. J. Dong, *Chem - Eur J* **2009**, *15*, 6116-6120.
[12] A. Ambrosi, A. Bonanni, Z. Sofer, J. S. Cross and M. Pumera, *Chem - Eur J* **2011**, *17*, 10763-10770.
[13] A. Bonanni, A. Ambrosi and M. Pumera, *Chem - Eur J* **2012**, *18*, 4541-4548.
[14] A. Bonanni, C. K. Chua, G. Zhao, Z. Sofer and M. Pumera, *ACS Nano* **2012**.
[15] A. Loo, A. Bonanni and M. Pumera, *Nanoscale* **2013**, *5*, 4758-4762.
[16] A. H. Loo, A. Bonanni and M. Pumera, *Chemelectrochem* **2015**, *2*, 743-747.
[17] J. H. Jung, D. S. Cheon, F. Liu, K. B. Lee and T. S. Seo, *Angew Chem Int Ed* **2010**, *49*, 5708-5711.
[18] H. Wang, Q. Zhang, X. Chu, T. Chen, J. Ge and R. Yu, *Angew Chem Int Ed* **2011**, *50*, 7065-7069.
[19] S. Roy, N. Soin, R. Bajpai, D. S. Misra, J. A. McLaughlin and S. S. Roy, *J Mater Chem* **2011**.
[20] L. Staudenmaier, *Ber Dtsch Chem Ges* **1898**, *31*, 1481-1487.
[21] W. S. Hummers and R. E. Offeman, *J Am Chem Soc* **1958**, *80*, 1339-1339.
[22] U. Hofmann and R. Holst, *Ber Dtsch Chem Ges* **1939**, *72*, 754-771.
[23] D. V. Kosynkin, A. L. Higginbotham, A. Sinitskii, J. R. Lomeda, A. Dimiev, B. K. Price and J. M. Tour, *Nature* **2009**, *458*, 872-U875.
[24] L. Escriva, G. Font and L. Manyes, *Food Chem Toxicol* **2015**, *78*, 185-206.
[25] M. Pascale, A. Visconti, M. Pronczuk, H. Wisniewska and J. Chelkowski, *J Sci Food Agic* **1997**, *74*, 1-6.
[26] A. Ambrosi and M. Pumera, *Chem - Eur J* **2013**, *19*, 4748-4753.
[27] M. Wu, R. Kempaiah, P. J. J. Huang, V. Maheshwari and J. W. Liu, *Langmuir* **2011**, *27*, 2731-2738.
[28] N. Varghese, U. Mogera, A. Govindaraj, A. Das, P. K. Maiti, A. K. Sood and C. N. R. Rao, *Chemphyschem* **2009**, *10*, 206-210.
[29] A. H. Loo, A. Bonanni and M. Pumera, *Nanoscale* **2012**, *4*, 143-147.
[30] A. E. Radi, J. L. A. Sanchez, E. Baldrich and C. K. O'Sullivan, *J Am Chem Soc* **2006**, *128*, 117-124.
[31] T. Szabo, O. Berkesi, P. Forgo, K. Josepovits, Y. Sanakis, D. Petridis and I. Dekany, *Chem Mater* **2006**, *18*, 2740-2749.
[32] C. Hontorialucas, A. J. Lopezpeinado, J. D. D. Lopezgonzalez, M. L. Rojascervantes and R. M. Martinaranda, *Carbon* **1995**, *33*, 1585-1592.
[33] S. F. Pei and H. M. Cheng, *Carbon* **2012**, *50*, 3210-3228.
[34] F. Malir, V. Ostry, A. Pfohl-Leszkowicz, J. Malir and J. Toman, *Toxins* **2016**, *8*, 1-50.